JOURNAL OF GUIDANCE, CONTROL, AND DYNAMICS
Vol. 30, No. 6, November–December 2007

Essentially Globally Asymptotically Stable Nutation Control Using a Single Reaction Wheel

Dale A. Lawrence*
University of Colorado, Boulder, Colorado 80309
and
Timothy E. Holden†
Ball Aerospace and Technology Corporation, Boulder, Colorado 80301

DOI: 10.2514/1.27790

Launch-vehicle volume and payload geometry often prefer a spacecraft design based on spin stabilization about a minor principal axis, at least for a portion of the spacecraft lifetime. Active stabilization is required to maintain minor-axis spin in the presence of energy dissipation. Lyapunov stability theory is used to develop a globally stable control law using a single reaction wheel mounted transverse to the desired spin axis. This control law provides practical automatic recovery of desired spin from any initial state, which linearized analysis and design methods cannot, including recovery from spin about a major axis (flat spin). A family of control laws is derived that includes linear feedback from a single rate gyro and a wheel tachometer.

I. Introduction

SPIN stabilization is one of the earliest methods of spacecraft attitude control. It provides a large angular momentum, making the vehicle resistant to attitude disturbances including torques from aerodynamic drag, solar pressure, gravity gradients, and magnetic moments. Except for dual-spin geosynchronous communication spacecraft [1] and some interplanetary missions [2], operational spin stabilization is seldom employed in modern large spacecraft. However, due to its simplicity and low cost, it is often used for many small-spacecraft missions (e.g., [3]) and in upper-stage-insertion segments of larger-spacecraft missions [4].

Classical treatments of rigid-body spin stability used momentum/energy polhodes in heuristic arguments [5,6] to demonstrate that with energy dissipation, simple spin is stable about a major principal axis and unstable about minor or intermediate principal axes. More recent analyses have provided validation, at least in cases in which energy dissipation can be well-characterized [7,8]. The rate of dissipation is a strong factor in the rate of convergence (divergence) of nutation about the major (minor) axes. Passive nutation-damping devices are often added to major-axis spinners to increase rates of dissipation, damping nutation more quickly. In some cases, active nutation damping [4] is employed to acquire operational nutation angles from launch-vehicle tipoff conditions in a sufficiently short time.

For minor-axis spinners, an active nutation-damping system is necessary for overall system stability in the presence of energy dissipation. This has been used for upper-stage orbit insertion, in which the vehicle is in minor-axis spin only until the kick motor is jettisoned, requiring relatively small amounts of gas-jet-actuator fuel. No spacecraft have been designed for operation in minor-axis spin, except, of course, for Explorer 1, for which the divergence into a major-axis (flat) spin instigated the classical analyses (e.g., [5,6]). Operational minor-axis spin would require reliable active nutation control laws. For long-lived missions, electric actuation (magnetic torque rods and reaction wheels) would be necessary.

Intermediate-axis spin also requires active control. This has been proposed using reaction wheels [9] and implemented using gas jets in a safe mode on the Lewis spacecraft.‡

Operational spin about a minor axis provides important advantages for some missions. Payload or instrument design may favor rotation about the long axis of the spacecraft. Available launch volumes, particularly as secondary payloads, may favor prolate mass properties. Finally, significant costs may be involved in adding ballast mass or locating components to guarantee oblate characteristics, particularly in a small-spacecraft program.

To be considered in a mission design, however, a prolate spinner must have a simple, reliable control law in which the stability properties are well-understood for spin originating in any state, including that of (flat) spin about the major axis.

This paper provides a Lyapunov design approach for constructing active nutation control laws using a single reaction wheel, mounted transverse to the desired spin axis, assumed to be the minor principal axis of inertia of the vehicle. Major-axis spin also can be treated, but the details are not reported here. This approach employs the full nonlinear equations of motion and results in a family of control laws that provide a specific type of global spin stability, producing reliable spin stabilization from any initial state. In particular, this approach enables operational minor-axis spin, using the reaction wheel to damp nutation and to provide automatic flat-spin recovery. In addition, the control laws are simple, using linear feedback of one rate gyro and a wheel tachometer.

Nutation-damping control laws have been designed using linearized equations of motion (see, for example, [9,10]). Other approaches consider the full nonlinear dynamics, but only provide local asymptotic stability (e.g., [11–13]). In both cases, stability is characterized only in a limited region about the desired spin state, and the extent of the stability region is difficult to ascertain. For a major-axis spinner, it may be possible to constrain operation close enough to the desired spin state. However, for a minor-axis spinner, the system is likely to initiate far from the desired spin equilibrium (e.g., during recovery from a flat spin). A global analysis is needed in this case.

Our work is distinguished from a large body of literature that addresses global behavior. Attitude control methods (e.g., [14–20])

Presented as Paper 4047 at the AIAA Guidance Navigation and Control, Denver, CO, 14–17 August 2000; received 14 September 2006; revision received 22 January 2007; accepted for publication 17 May 2007.

*Associate Professor, Department of Aerospace Engineering Sciences. Senior Member AIAA.

†Advanced Systems Manager, Operational Space.

‡Data available online at http://arioch.gsfc.nasa.gov/300/html/lewis_document.pdf [retrieved 20 July 2007].

seek zero angular velocity, which results in loss of dynamic coupling and corresponding controllability, compared with the spinning equilibria considered here. Angular velocity control methods can be divided into two main classes: detumble/despin and nutation control. The former (see [21–29]) also reduces rotational kinetic energy to zero and is not useful in spin stabilization. In nutation control, simple spin about a desired spacecraft body axis is the objective. Many approaches have been used [21–23,30–34] in which the spacecraft is treated as a rigid body to which external control torques are applied (e.g., via magnetic torque rods or gas jets). No internal momentum storage is considered. The first can be limited by the orientation and strength of the external magnetic field, and the second is limited by onboard fuel capacity. We consider control torque supplied by a reaction wheel, for which mission life is limited only by onboard electrical-power-generation capability. Translating masses [10] and control moment gyros have also been used [28]. Reaction-wheel actuation provides internal torques that arise from changing the angular momentum of the wheel. Internal momentum storage produces additional state variables in the spacecraft dynamics. Actually, three wheels aligned with the spacecraft principal axes can be modeled as a rigid body with external torques [35]. Other approaches have used two wheels [36].

Here, we investigate nutation control using a single reaction wheel, mounted transverse to the desired spin axis. One widely reported result [35,37–40] uses nonlinear feedback of the product of two angular velocities, a reaction wheel aligned with the minor or major axis, and provides neutral stability about the intermediate axis in the absence of energy dissipation. Local asymptotic stability to simple spin is provided by the addition of a dissipation law, requiring measurement of the three-axis-body rate and relative wheel-body speed [11,12]. Global asymptotic stability is provided if external three-axis damping torques are assumed, together with a second actuator to cancel damping in the desired spin axis [41]. In contrast, our approach provides a type of global asymptotic stability, in which final spin about either the major or minor axis can be selected, using linear feedback of one angular velocity sensor and a relative wheel-speed sensor (tachometer). Principal-axis alignment of the wheel and external damping torque are not required. Other one-actuator nutation control schemes [21–23,30–32] do not consider reaction-wheel dynamics.

This paper is organized as follows. Nonlinear dynamics of the spacecraft bus with an added reaction wheel are reviewed in Sec. II, along with the transverse-wheel-mounting constraint. Section III introduces Lyapunov functions for these dynamics that demonstrate asymptotic stability of the equilibrium spin in both the passive and active cases. Details are provided in Appendices A, B, C, and D. Section IV illustrates closed-loop behavior, including flat-spin recovery, with simulation examples.

II. Spacecraft Dynamics

It is convenient to express the spacecraft dynamics in a rather unusual form (compared with, for example, [42]), isolating the angular momentum due to inertial (rather than relative) wheel spin. The general formulation can be found in [43]. Here, the wheel spin axis is oriented transverse to the desired spacecraft spin axis. This restriction permits a precise theoretical treatment, but is less restrictive than other single-wheel nutation control approaches [14,35]. Simulations (Sec. IV) indicate that performance is not sensitive to wheel misalignment.

Figure 1 shows two spacecraft body frames and a reaction wheel. The bus has mass m_b, center of mass at o_b, and moment-of-inertia tensor about o_b designated by $\mathbf{I}_b^{o_b}$, with principal moments of inertia A', B', and C' and corresponding principal body frame $F' = (\hat{\mathbf{1}}', \hat{\mathbf{2}}', \hat{\mathbf{3}}')$.

The wheel is axisymmetric, with mass m_w, center of mass o_w, and moment-of-inertia tensor $\mathbf{I}_w^{o_w}$ about o_w, with principal moments of inertia K, L, and L, and corresponding principal wheel frame $\hat{\mathbf{a}}$, $\hat{\mathbf{t}}_1$, and $\hat{\mathbf{t}}_2$, where $\hat{\mathbf{a}}$ is the rotation axis of the wheel, and $\hat{\mathbf{t}}_1$ and $\hat{\mathbf{t}}_2$ are any pair of orthogonal transverse axes.

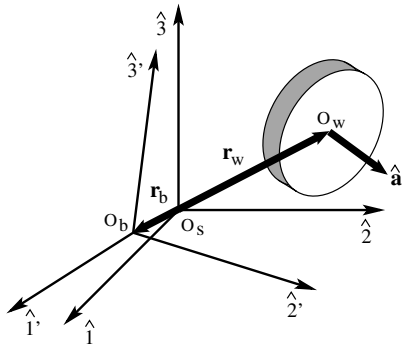

Fig. 1 Wheel placement relative to the bus (primed) and spacecraft (unprimed) principal axes.

The wheel is mounted in the bus with the center of mass at o_w. The spacecraft now has center of mass o_s, which is offset from the bus center of mass by $\mathbf{r}_b$, and the wheel is centered at $\mathbf{r}_w$ relative to o_s, where $m_w\mathbf{r}_w + m_b\mathbf{r}_b = \mathbf{0}$. Using dyadic notation [44] with $\mathbf{I}$ indicating the unit tensor, the moment-of-inertia tensor of the bus about the spacecraft center of mass o_s is $\mathbf{I}_b^{o_s} = \mathbf{I}_b^{o_b} + m_b(r_b^2\mathbf{I} - \mathbf{r}_b\mathbf{r}_b)$, and the moment-of-inertia tensor of the wheel about o_s is $\mathbf{I}_w^{o_s} = \mathbf{I}_w^{o_w} + m_w(r_w^2\mathbf{I} - \mathbf{r}_w\mathbf{r}_w)$.

The total inertial angular momentum vector of the spacecraft about o_s is then given by [43]

$$\mathbf{h} = \mathbf{I}_b^{o_s}\cdot\boldsymbol{\omega}_b + m_w\left(r_w^2\mathbf{I} - \mathbf{r}_w\mathbf{r}_w\right)\boldsymbol{\omega}_b + \mathbf{I}_w^{o_w}\cdot\boldsymbol{\omega}_w \tag{1}$$

where $\boldsymbol{\omega}_b$ and $\boldsymbol{\omega}_w$ are the angular velocity vectors of the bus and wheel, respectively, with respect to an inertial frame. If the wheel has rotation speed u relative to the bus,

$$\boldsymbol{\omega}_w = \boldsymbol{\omega}_b + u\hat{\mathbf{a}} \tag{2}$$

Define the inertial wheel speed Ω via

$$\Omega = \boldsymbol{\omega}_w\cdot\hat{\mathbf{a}} = \boldsymbol{\omega}_b\cdot\hat{\mathbf{a}} + u \tag{3}$$

Using these velocity expressions in Eq. (1) and collecting terms

$$\mathbf{h} = \left[\mathbf{I}_b^{o_s} + \mathbf{I}_w^{o_w} + m_w\left(r_w^2\mathbf{I} - \mathbf{r}_w\mathbf{r}_w\right) - \mathbf{I}_w^{o_w}\cdot\hat{\mathbf{a}}\,\hat{\mathbf{a}}\right]\boldsymbol{\omega}_b + \mathbf{I}_w^{o_w}\cdot\hat{\mathbf{a}}\,\hat{\mathbf{a}}\,\Omega \tag{4}$$

Because, by definition, $\hat{\mathbf{a}}$ is a principal axis of $\mathbf{I}_w^{o_w}$, the spacecraft angular momentum can be written in the form

$$\mathbf{h} = \mathbf{I}_B\cdot\boldsymbol{\omega}_b + K\Omega\hat{\mathbf{a}} \tag{5}$$

where $\mathbf{I}_w^{o_w}\cdot\hat{\mathbf{a}} = K\hat{\mathbf{a}}$ and we define

$$\mathbf{I}_B = \mathbf{I}_b^{o_s} + \mathbf{I}_w^{o_w} + m_w\left(r_w^2\mathbf{I} - \mathbf{r}_w\mathbf{r}_w\right) - K\hat{\mathbf{a}}\,\hat{\mathbf{a}} = \mathbf{I}_b^{o_s} + \mathbf{I}_w^{o_s} - K\hat{\mathbf{a}}\,\hat{\mathbf{a}} \tag{6}$$

The first term in Eq. (5) is the angular momentum component of the spacecraft with zero inertial wheel speed Ω, and the second term is the spacecraft momentum component due to inertial wheel spin alone [43].

Use $\mathbf{I}_B$ from Eq. (6) to define principal body-frame F axes $(\hat{\mathbf{1}}, \hat{\mathbf{2}}, \hat{\mathbf{3}})$ and corresponding principal moments of inertia A, B, and C so that

$$\mathbf{I}_B = A\hat{\mathbf{1}}\,\hat{\mathbf{1}} + B\hat{\mathbf{2}}\,\hat{\mathbf{2}} + C\hat{\mathbf{3}}\,\hat{\mathbf{3}} \tag{7}$$

The $\hat{\mathbf{3}}$ axis is designated as the desired spin axis. Note that $\hat{\mathbf{a}}$ need not be a principal axis of $\mathbf{I}_b^{o_s}$, as in [35], and the offset vector $\mathbf{r}_w$ need not be colinear with the wheel spin axis, as in [14]. However, we will specialize the wheel mounting (in Sec. III.B) so that $\hat{\mathbf{a}}$ is transverse to the desired spin axis (i.e., the free vector $\hat{\mathbf{a}}$ will be assumed to lie in the $\hat{\mathbf{1}}$–$\hat{\mathbf{2}}$ plane). Define θ as the rotation angle (about the $\hat{\mathbf{3}}$ axis) of the wheel spin axis $\hat{\mathbf{a}}$ relative to the $\hat{\mathbf{1}}$ axis (see Fig. 2).

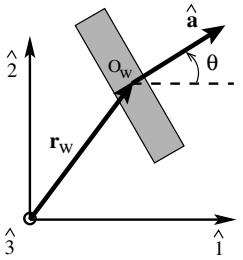

Fig. 2 Wheel spin-axis orientation, restricted to the $\hat{\mathbf{1}}$–$\hat{\mathbf{2}}$ plane.

Because the addition of the wheel changes the spacecraft principal axes, it is generally difficult to determine a physical mounting for the wheel and spin-axis orientation to achieve a prespecified alignment angle θ. Fortunately, particular values for θ are not needed. To ensure that $\hat{\mathbf{a}}$ lies in the $\hat{\mathbf{1}}$–$\hat{\mathbf{2}}$ plane, it is sufficient to place the wheel c.g. and its spin axis in the bus $\hat{\mathbf{1}}'$–$\hat{\mathbf{2}}'$ plane, because this results in $\hat{\mathbf{3}}' = \hat{\mathbf{3}}$. Another approach is to center the wheel on the $\hat{\mathbf{3}}'$ axis, with $\hat{\mathbf{a}}$ perpendicular to $\hat{\mathbf{3}}'$. If ballast masses are also used, the wheel can be mounted anywhere in the spacecraft, with the spin axis oriented orthogonal to the $\hat{\mathbf{3}}'$ axis.

With zero external torques, the spacecraft dynamics are described by

$$\mathbf{0} = \frac{{}^{I}\mathrm{d}}{\mathrm{d}t}\mathbf{h} = \frac{{}^{F}\mathrm{d}}{\mathrm{d}t}\mathbf{h} + \boldsymbol{\omega}_b \times \mathbf{h} \tag{8}$$

where I indicates an inertial-frame derivative. Substituting Eq. (5) for $\mathbf{h}$ and defining $\dot{\boldsymbol{\omega}}_b$ as the body-frame F derivative produces

$$\frac{{}^{F}\mathrm{d}}{\mathrm{d}t}\boldsymbol{\omega}_b \equiv \dot{\boldsymbol{\omega}}_b = -\mathbf{I}_B^{-1} \cdot [\boldsymbol{\omega}_b \times (\mathbf{I}_B \cdot \boldsymbol{\omega}_b + K\Omega\hat{\mathbf{a}}) + K\dot{\Omega}\,\hat{\mathbf{a}}] \tag{9}$$

If the wheel is acted on by an internal motor torque τ about the spin axis $\hat{\mathbf{a}}$ resulting from a voltage-fed permanent-magnet dc motor [45], we also have

$$K\dot{\Omega} = \tau = -\frac{N^2}{R}u + \frac{N}{R}e \tag{10}$$

where N [N · m/A] is the motor torque constant, R [Ω] is the armature resistance, and e is the control (input) voltage. The motor rotor is included in the mass properties of the wheel, and the stator is incorporated into the spacecraft mass properties. Together, Eqs. (9) and (10) describe the spacecraft dynamics. It is convenient to use inertial velocity Ω for stability analysis, but relative velocity u is more easily measured for feedback control.

III. Lyapunov Control for Global Spin Stability

We first consider the passive case (zero control input) in which the back electromotive force (EMF) in the motor provides energy loss that results in a rigorous proof of major-axis spin stability. Active control using feedback from one rate gyro and a wheel tachometer is then presented.

A. Passive Spin Stability

Assumptions:

1) No external torques act on the spacecraft.

2) The wheel spin axis $\hat{\mathbf{a}}$ is not a symmetry axis of the locked-rotor mass properties $\mathbf{I}_b^{o_s} + \mathbf{I}_w^{o_s}$.

3) The wheel is actuated by a voltage-fed permanent-magnet dc motor.

Theorem 1: For passive spin under Assumptions 1–3, if the motor voltage is zero, angular velocity is *essentially globally asymptotically stable* to simple spin about the major axis of the locked-rotor mass properties $\mathbf{I}_b^{o_s} + \mathbf{I}_w^{o_s}$.

Proof: The spacecraft kinetic energy T is given by [43]

$$T = \tfrac{1}{2}(\boldsymbol{\omega}_b \cdot \mathbf{I}_B \cdot \boldsymbol{\omega}_b + K\Omega^2) \tag{11}$$

and it is straightforward to show that

$$\dot{T} = K\dot{\Omega}u = -\frac{N^2}{R}u^2 + \frac{N}{R}ue \tag{12}$$

Thus, for zero input voltage e, energy is dissipated through the back EMF damping in the motor and $\dot{T} \le 0$. Because T is nonnegative, T converges, and because T is radially unbounded, $\boldsymbol{\omega}_b$ and Ω are bounded. From Eqs. (3), (9), and (10), this implies that u and hence $\dot{T}$ are uniformly continuous, and by the Barbalat Lemma [46], $\dot{T}$ converges to zero, as does u. By Eq. (10), $\dot{\Omega}$ also converges to zero. Thus, the spacecraft dynamics converge to the locked-rotor condition, where $\Omega = \boldsymbol{\omega}_b \cdot \hat{\mathbf{a}}$ and

$$T = \tfrac{1}{2}\boldsymbol{\omega}_b \cdot \left(\mathbf{I}_b^{o_s} + \mathbf{I}_w^{o_s} - K\hat{\mathbf{a}}\,\hat{\mathbf{a}} + K\hat{\mathbf{a}}\,\hat{\mathbf{a}}\right) \cdot \boldsymbol{\omega}_b = \tfrac{1}{2}\boldsymbol{\omega}_b \cdot \left(\mathbf{I}_b^{o_s} + \mathbf{I}_w^{o_s}\right) \cdot \boldsymbol{\omega}_b \tag{13}$$

where $\mathbf{I}_b^{o_s} + \mathbf{I}_w^{o_s}$ is the spacecraft locked-rotor moment-of-inertia tensor, with principal moments of inertia $\bar{A}$, $\bar{B}$, and $\bar{C}$. Hence, the spacecraft with zero-voltage rotor and the locked-rotor rigid body have the same set of asymptotic solutions.

For asymmetric mass properties $\bar{A} \neq \bar{B} \neq \bar{C}$, there are six isolated equilibria for each initial momentum magnitude h_o given by simple spin about each of the principal axes with corresponding rates $\pm h_o/A$, $\pm h_o/B$, and $\pm h_o/C$. For symmetric spacecraft, any spin normal to the axis of symmetry is an equilibrium, along with spin about the symmetry axis. Nonequilibrium solutions $\boldsymbol{\omega}_b$ to the rigid body [Eq. (13)] for constant T are well known [47–49] to be Jacobian elliptic functions that result in $\boldsymbol{\omega}_b$ coning about either the major or minor principal axis of $\mathbf{I}_b^{o_s} + \mathbf{I}_w^{o_s}$ or heteroclinic motion on a separatrix connecting intermediate-axis spin equilibria. Now $\dot{\Omega} = \dot{\boldsymbol{\omega}}_b \cdot \hat{\mathbf{a}}$ will not converge to zero unless 1) $\boldsymbol{\omega}_b$ converges to an equilibrium (becomes constant), 2) $\boldsymbol{\omega}_b$ converges to circular coning motion around $\hat{\mathbf{a}}$ with constant cone axis, or 3) $\boldsymbol{\omega}_b$ converges to a rigid-body separatrix that is orthogonal to $\hat{\mathbf{a}}$. Separatrix motion converges to intermediate-axis spin, making option 3 equivalent to option 1. Coning motion for option 2 does not have a constant cone axis (the *dn* Jacobian elliptic function) unless the mass properties are symmetric, and $\hat{\mathbf{a}}$ is aligned with the symmetry axis of $\mathbf{I}_b^{o_s} + \mathbf{I}_w^{o_s}$, violating Assumption 2. Thus, motion converges to one of the simple spin-equilibrium conditions.

The lowest-energy equilibrium is spin about the major axis. If the spacecraft begins with an initial value for T lower than the value associated with locked-rotor intermediate-axis spin, then motion can only converge to major-axis equilibrium spin, showing that major-axis spin is locally asymptotically stable. When higher initial energies are present, convergence to spin about the intermediate axis or even the minor axis cannot be ruled out mathematically, but these equilibria are unstable, as shown in Appendix A. Hence, to converge to these equilibria, state trajectories must remain on thin stable manifolds leading to the equilibria, which could not occur in the presence of disturbances such as cogging torques in the reaction-wheel motor. Thus, we have *essential global asymptotic stability*, because we have global asymptotic stability to major-axis spin, except for states on the thin stable manifolds leading to intermediate- or minor-axis equilibria. □

Although this result is weaker than conventional global asymptotic stability, the distinction is purely mathematical; torque disturbances in practice prevent exact stable manifold motion, resulting in eventual major-axis spin. Unfortunately, the rate of energy loss can be quite small. Also, the passive case does not provide a means to damp nutation about the minor axis for stabilizing prolate spin. The main results of this paper use active feedback control of motor voltage e to provide more aggressive nutation damping, which can produce essential global stability of *minor*-axis spin. More aggressive nutation damping for major-axis spin can also be produced, although this case is not treated here (see [50] for initial results for both prolate and oblate spins).

B. Active Spin Stability

Under active control, the desired equilibrium is

$$\boldsymbol{\omega}_b = \omega_o \hat{\mathbf{3}}, \qquad \Omega = 0 \tag{14}$$

for some spin rate ω_o, that is, simple spin (no nutation) about the $\hat{\mathbf{3}}$ axis with zero inertial wheel spin. Because the wheel is transverse to the $\hat{\mathbf{3}}$ axis, Eq. (3) also implies zero relative wheel spin u. Stability of a *set* of $\hat{\mathbf{3}}$-axis spins is of interest, rather than stability of a particular equilibrium along this line. Because external torques are zero, the initial vehicle angular momentum magnitude $h = |\mathbf{h}|$ is a constant of the motion, which constrains the system states to evolve on a three-dimensional cylindrical submanifold of $\Re^4$. This is cylindrical because changes in wheel momentum and one component of body momentum can cancel, resulting in no change to the total spacecraft momentum. Boundedness of wheel spin is therefore an important question to be addressed by stability analysis, as well as the convergence of spacecraft states to the desired equilibrium spin. When this convergence occurs, the system is termed semistable [51], or partially stable [52], because the initial spacecraft momentum determines the equilibrium spin velocity $\omega_o = \pm\sqrt{h^2/C^2}$, and asymptotic stability occurs in only part of the state space (i.e., the subspace normal to the $\hat{\mathbf{3}}$ axis).

Assumptions:

4) The wheel is mounted with spin axis $\hat{\mathbf{a}}$ orthogonal to the spacecraft $\hat{\mathbf{3}}$ axis.

5) If the mass properties are asymmetric ($A \neq B$), then the wheel spin axis $\hat{\mathbf{a}}$ is not aligned with the major axis of $\mathbf{I}_B$.

Theorem 2: For minor-axis spin under Assumptions 1–5, if the control parameter $\Gamma^2 > C|B - A|$, then the rigid spacecraft [Eqs. (9) and (10)] with prolate mass properties $A > C$ and $B > C$, containing a single reaction wheel under feedback [Eq. (20)] from a wheel tachometer and one rate gyro, is *essentially globally asymptotically stable* to simple spin about the $\hat{\mathbf{3}}$ axis.

Proof: Consider the quadratic Lyapunov function candidate

$$V = [(\mathbf{I}_B - \mathbf{I}_C)\cdot\boldsymbol{\omega}_b + K\Omega\hat{\mathbf{a}}]\cdot\mathbf{M}\cdot[(\mathbf{I}_B - \mathbf{I}_C)\cdot\boldsymbol{\omega}_b + K\Omega\hat{\mathbf{a}}] + K^2\Gamma^2\Omega^2 \tag{15}$$

where $\mathbf{M}$ is positive semidefinite, $\mathbf{I}_C = C\mathbf{I}$, and Γ is an arbitrary constant. Note that

$$\mathbf{I}_B - \mathbf{I}_C = (A - C)\hat{\mathbf{1}}\hat{\mathbf{1}} + (B - C)\hat{\mathbf{2}}\hat{\mathbf{2}} + (0)\hat{\mathbf{3}}\hat{\mathbf{3}} \tag{16}$$

hence, V does not depend on the $\hat{\mathbf{3}}$-axis component of $\boldsymbol{\omega}_b$. For the limiting wheel inertia case $K = 0$, and M as given in Eq. (17), this Lyapunov function reduces to the Lyapunov function used in [53,54] for rigid-body stability analysis and in [55] for design of magnetic nutation-damping systems.

When the desired spin axis $\hat{\mathbf{3}}$ is the minor axis, we have $A > C$ and $B > C$. As shown in Appendix B, taking the time derivative of Eq. (15) and substituting the equations of motion (9) and (10) and

$$\mathbf{M} = A(B - C)\hat{\mathbf{1}}\hat{\mathbf{1}} + B(A - C)\hat{\mathbf{2}}\hat{\mathbf{2}} + (0)\hat{\mathbf{3}}\hat{\mathbf{3}} \tag{17}$$

results in

$$\dot{V} = 2K\dot{\Omega}[(C\delta + \gamma)\boldsymbol{\omega}_b\cdot\hat{\mathbf{a}} + \gamma u] \tag{18}$$

where $\dot{\Omega}$ depends on the control signal e from Eq. (10) and δ and γ are constants:

$$\delta = (A - C)(B - C)$$
$$\gamma = K[C(B - C)\cos^2\theta + C(A - C)\sin^2\theta + \Gamma^2] \tag{19}$$

Employ a control law such that

$$e = -f\{(C\delta + \gamma)\boldsymbol{\omega}_b\cdot\hat{\mathbf{a}} + \gamma u\} + Nu \tag{20}$$

where f is any definite odd function [i.e., $\text{sign}(f\{x\}) = \text{sign}(x)$ and $f\{x\} = 0$ implies $x = 0$]. This control law produces a $K\dot{\Omega}$ in Eq. (10) that ensures that V is monotone decreasing:

$$\dot{V} = -2\frac{N}{R}f\{(C\delta + \gamma)\boldsymbol{\omega}_b\cdot\hat{\mathbf{a}} + \gamma u\}[(C\delta + \gamma)\boldsymbol{\omega}_b\cdot\hat{\mathbf{a}} + \gamma u] \leq 0 \tag{21}$$

Note that the control law (20) only requires a single rate-gyro sensor, aligned with the wheel axis $\hat{\mathbf{a}}$, and a tachometer on the wheel measuring relative speed u. In its simplest form, Eq. (20) is linear in the measured quantities.

Because V is nonnegative and $\dot{V}$ is nonpositive from Eq. (21), V converges. Note that when $\Gamma^2 > 0$, V is radially unbounded for all $\boldsymbol{\omega}_b$ and Ω, except those in the subspace spanned by the vector $(\hat{\mathbf{3}}, 0)$. The total angular momentum constraint bounds the component of $\boldsymbol{\omega}_b$ along $\hat{\mathbf{3}}$. Hence, the angular velocities $\boldsymbol{\omega}_b$ and Ω are bounded, and from Eqs. (3), (9), and (10), $\dot{V}$ is uniformly continuous. By the Barbalat Lemma [46], $\dot{V}$ converges to zero, and angular velocities converge to the set $P \in \Re^4$, where $\dot{V} = 0$. In fact, using the LaSalle invariance principle [46], we have convergence within $\dot{V} = 0$ to the largest subset S, which also satisfies the equations of motion. Then $S \subset P \in \Re^4$ is an invariant set of Eqs. (9) and (10), because motion originating in S remains in S.

As shown in Appendix C, when $\Gamma^2 > 0$, the invariant set S under feedback control consists of six equilibrium points (even in the symmetric case, in which $A = B$). Two are located at $\pm\omega_o$ along the $\hat{\mathbf{3}}$ axis and constitute the desired (minor-axis) spin states. Four other (undesired) equilibria exist in S, which would be a concern except that these equilibria are unstable, as shown in Appendix D. Thus, these equilibria each have an unstable manifold dimension of at least one, along which states move away from the equilibrium. In the three-dimensional manifold of constant momentum magnitude, a submanifold can also exist that attracts states toward the undesired equilibrium, but this stable manifold can have a dimension no larger than two. As a result, initial states that are attracted to an undesired equilibrium must originate on thin sets, and all other initial conditions (i.e., except for these sets of measure zero) result in the desired equilibrium spin. The set of two desired equilibria are then *essentially globally asymptotically stable*. □

As mentioned earlier, this result is mathematically weaker than *global asymptotic stability*, but it provides practical recovery from any initial spin state to the desired equilibria, because measurement noise in the control system or wheel torque disturbances prevent the system from remaining on any of these thin sets leading to the undesired equilibria.

The next section illustrates the behavior produced by the Lyapunov control law on two worst-case examples. One considers the scenario in which the spacecraft state is initialized on one of the undesired equilibria. The second case explores behavior in recovering stable prolate spin from a flat (oblate) spin. Robustness of the control law is indicated by a third example, which shows that the closed-loop behavior is not sensitive to wheel misalignment and mass-property uncertainty.

IV. Simulation Examples

The first two simulations are for a prolate spinner with the following mass properties: bus mass $m_b = 72$ kg, with principal moments of inertia ($\text{kg}\cdot\text{m}^2$) of $A' = 8.1600$, $B' = 6.9600$, and $C' = 4.5600$; wheel mass $m_w = 2.4127$ kg, with center of mass o_w located in the $\hat{\mathbf{1}}'$–$\hat{\mathbf{2}}'$ plane, at an angle of $\pi/3$ rad from the $\hat{\mathbf{1}}'$ axis, and at a distance of 0.15 m from the bus center of mass o_b. The spin axis $\hat{\mathbf{a}}$ lies in the $\hat{\mathbf{1}}$–$\hat{\mathbf{2}}$ plane, at an angle of 0.4189 rad about the $\hat{\mathbf{3}}$ axis from the $\hat{\mathbf{1}}$ axis. The wheel has principal moments of inertia ($\text{kg}\cdot\text{m}^2$) of $K' = 0.0077$ and $L' = 0.0054$. This wheel mounting satisfies Assumption 4. Using the procedure outlined in Sec. II, we obtain an $\mathbf{I}_B$ with principal moments of inertia ($\text{kg}\cdot\text{m}^2$) of $A = 8.1942$, $B = 6.9718$, and $C = 4.6130$ and a wheel-alignment angle θ (see Fig. 2) relative to the spacecraft principal frame of 0.4398 rad; this

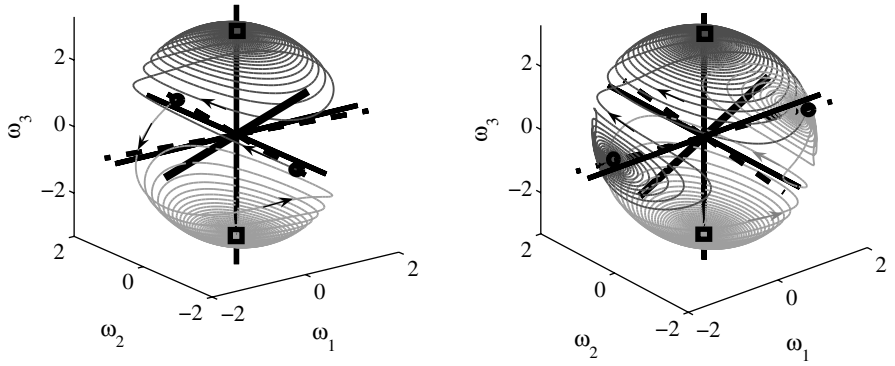

Fig. 3 Oblique view of bus angular velocity ω_b trajectory under a Lyapunov control law, beginning on undesired equilibria. Solid lines are the principal axes of $\mathbf{I}_B$, and dashed lines are the loci of undesired equilibria, which lie in the $\hat{\mathbf{1}}$–$\hat{\mathbf{2}}$ plane. The reaction-wheel spin axis (thick line) also lies in this plane.

satisfies Assumption 5. The control parameter $\Gamma^2 = 100$ (larger than $C|B - A| = 5.6389$), and this results in the parameter $\gamma = 0.8640$. The control law is a linear version of Eq. (20):

$$e = -\kappa\{(C\delta + \gamma)\boldsymbol{\omega}_b \cdot \hat{\mathbf{a}} + \gamma u\} + Nu \tag{22}$$

where feedback gain $\kappa = 0.01$. The simulation was initialized near each of the four undesired closed-loop equilibria given by Eqs. (C2), (C3), (C9), and (C10), and Fig. 3 shows the resulting evolution of the angular velocity $\boldsymbol{\omega}_b$ in components relative to the $(\hat{\mathbf{1}}, \hat{\mathbf{2}}, \hat{\mathbf{3}})$ frame. The left side of Fig. 3 shows initializations resulting from equilibrium parameterizations $c_1 = -0.9150$, $c_2 = 0.6422$, and $\sigma_2 = \pm 1.8$ from Appendix C. The right side results from $c_1 = -0.9150$ and $c_2 = -1.5572$, with $\sigma_2 = \pm 1.0$. All four undesired equilibria have a zero $\hat{\mathbf{3}}$ component of angular velocity ($\sigma_3 = 0$). The initial states are marked with a circle, and the final states are marked with a rectangle, showing that in each case, the trajectory converges to simple $\hat{\mathbf{3}}$-axis spin, as proved in Theorem 2. Note that the sign of the final spin depends on how the state trajectory leaves the unstable equilibrium, which depends on how numerical simulation errors accumulate. Additional steps must be taken in the control law to assure a desired sign in the final spin.

Figure 4 shows the angular velocity components versus time for one of these four initial condition cases. The states remain near the undesired equilibria for approximately 200 s before numerical disturbances result in deviation from the thin stable manifold, resulting in rapid repulsion from this unstable equilibrium and transition to prolate spin at about 400 s. Simulation errors have a role similar to disturbance torques in practice, causing the system state to deviate from the stable manifolds, leading to undesired equilibria. Note that ω_1, ω_2, and Ω converge to zero, and ω_3 converges to approximately -3.17 rad/s in a stable prolate spin. Figure 5 shows that the corresponding Lyapunov function is monotone decreasing toward zero. The total kinetic energy is decreased by about 10 J by the motor and control law to its final value at the minor-axis spin equilibrium. Peak motor torque during the transition is approximately 0.2 N · m. Peak motor mechanical power is less than 5 W, with an rms mechanical power provided by the motor over the approximately 300-s transition of only about 0.25 W. Total angular momentum magnitude is constant (except for numerical simulation errors), because there are no external torques; variational integration may be applied to improve these errors (see, for example, [56]). A wide variation in recovery time is possible by varying the feedback gain κ, although larger gains require larger motor peak torque and correspondingly larger power-source capabilities.

The angular velocity in this example is qualitatively similar to a rigid body with energy dissipation, although we have asymptotic stability of the *minor* axis here. The dashed undesired equilibria lines in Fig. 3 (left side) have angular velocity motion about them, which is characteristic of a rigid-body intermediate axis with a saddle-point equilibrium. The dashed undesired equilibria on the right side of Fig. 3 exhibit unstable spiral behavior that is characteristic of dissipative spin about a rigid-body minor axis. The effect of the Lyapunov control law is therefore a small rotation of the equilibrium lines (relative to the rigid-body principal axes), together with a swapping of the stability properties of the major and minor-axis spins. Because the effective mass properties are not significantly affected by the control law and the total momentum is not changed, stabilization is accomplished with little energy expenditure.

The second example illustrates flat-spin recovery using the same values for the control parameters Γ and κ as those already shown. Initial conditions lie on the locked-rotor major axis, which is the essentially globally asymptotically stable equilibrium of the spacecraft in the passive state, in which the applied wheel voltage e is

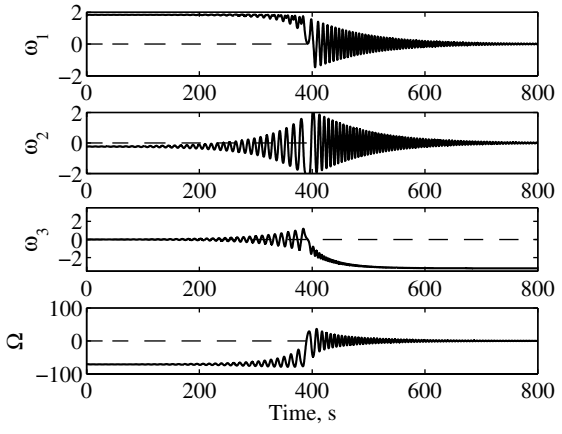

Fig. 4 Angular velocities (rad/s) beginning on an undesired equilibrium of the closed-loop Lyapunov control system.

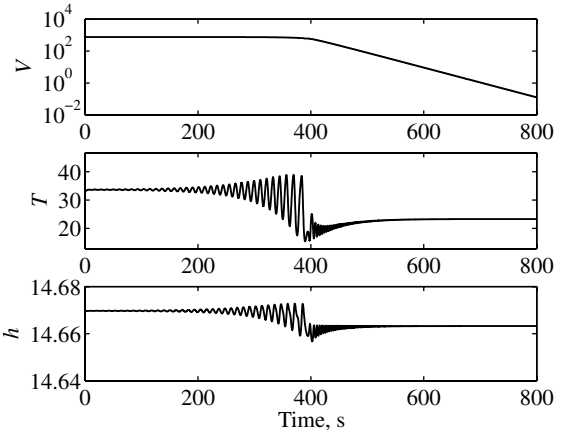

Fig. 5 Lyapunov function V, kinetic energy T (J), and total angular momentum magnitude $|h|$ (N · m · s) beginning on an undesired equilibrium.

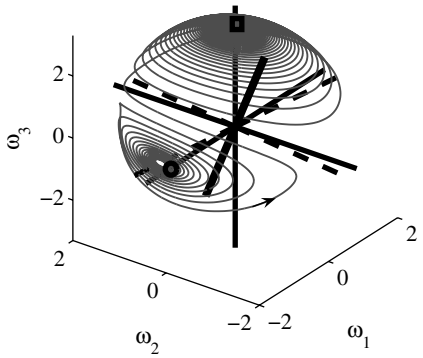

Fig. 6 Oblique view of flat-spin recovery under a Lyapunov control law. Solid lines are the locked-rotor $\mathbf{I}_b^{o_s} + \mathbf{I}_w^{o_s}$ principal axes, and dashed lines are the locus of undesired equilibria.

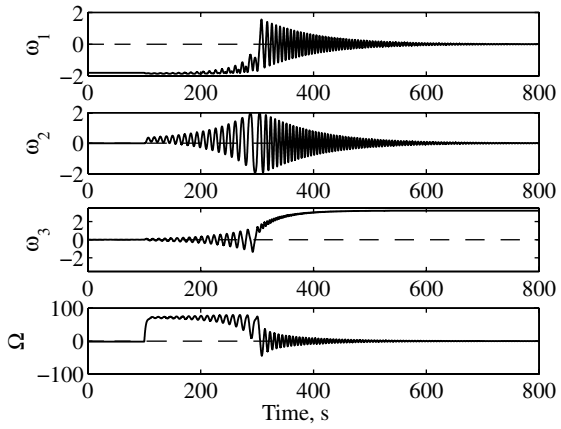

Fig. 7 Angular velocities during flat-spin recovery (rad/s).

zero. This condition is simulated for 100 s, at which point the Lyapunov control law is enabled. Figure 6 shows the resulting trajectory for the bus angular velocity components, beginning at a passive equilibrium (circle) on the locked-rotor major axis (solid line) and converging to ω_1, ω_2, and Ω equal zero (rectangle). Because the passive equilibrium is not on an equilibrium of the closed-loop system (dashed lines), the angular velocities immediately diverge from major-axis spin when the control law is enabled and quickly converge to the desired minor-axis spin. Figure 7 shows the velocity components of the bus and wheel versus time. Figure 8 shows the corresponding Lyapunov function V (monotone decreasing) and the total kinetic energy T. The kinetic energy has a larger final value due to the higher energy in minor-axis spin. Total angular momentum is once again conserved (except for numerical errors).

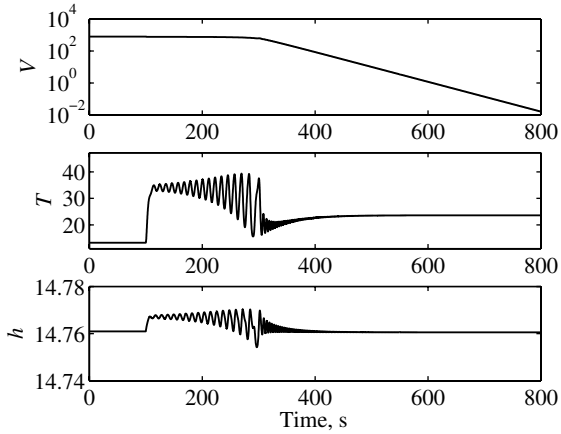

Fig. 8 Lyapunov function V, kinetic energy T (J), and total angular momentum magnitude h (N · m · s) for flat-spin recovery.

A potential difficulty with flat-spin recovery occurs when the locked-rotor major axis is aligned with an undesired equilibria line (e.g., solid lines in Fig. 6 align with the dashed lines). This produces behavior similar to the case in Fig. 3, in which divergence from this initial state will eventually occur because it is unstable, but it may be difficult to predict how long this will take. As shown in Appendix C, this condition can be avoided by locating or orienting the wheel so that undesired equilibria do not lie on the locked-rotor principal axes, providing immediate divergence from flat spin when the control law is enabled.

The third example investigates the robustness of the control law to mass-property uncertainty and wheel-misalignment errors, which are larger than would be expected from modern CAD models of spacecraft. The spacecraft and wheel are the same as in the previous examples, but the wheel center is elevated 20 deg above the $\hat{\mathbf{1}}'$–$\hat{\mathbf{2}}'$ plane and its spin axis is tilted 10 deg out of this plane. This results in a wheel axis tilt of 9.75 deg out of the plane transverse to the desired spin axis, violating Assumption 3. In addition, the control law uses mass properties that are in error as follows: A is 10% too large, B is 5% too small, C is 8% too large, and the mounting angle θ is 10% too small. The control law parameters Γ and κ are the same as before. Figure 9 shows the resulting trajectory of body angular velocities, starting at a flat-spin condition for these mass properties. After 100 s of zero motor voltage, the Lyapunov control law is enabled, producing stable prolate spin that is very similar to the exact mass properties and wheel-alignment case of flat-spin recovery in Fig. 6. Figure 10 indicates that the wheel velocity Ω does not go to zero, due to its nonzero component in the desired spin direction. Accordingly, the Lyapunov function V remains bounded away from zero, as seen in Fig. 11. Similar subtle differences were observed in other simulations with differing wheel-alignment and mass-property errors and different initial conditions. A comprehensive robustness study is beyond the scope of the paper, but these results indicate that

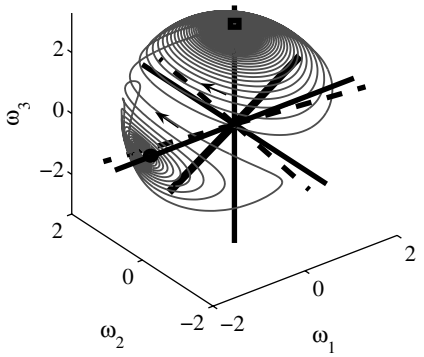

Fig. 9 Oblique view of flat-spin recovery under a Lyapunov control law, with wheel-misalignment and mass-property errors in the control law.

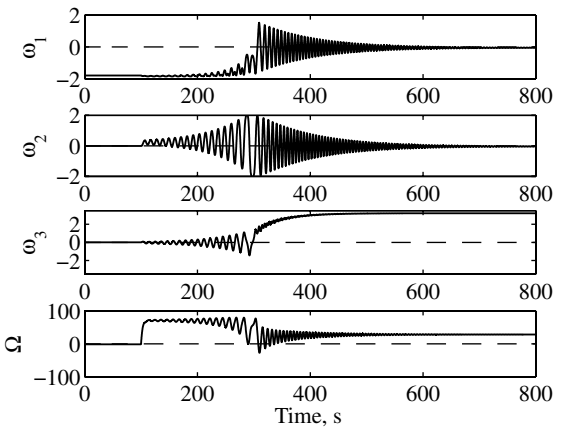

Fig. 10 Angular velocities during flat-spin recovery with mass-property and alignment errors (rad/s).

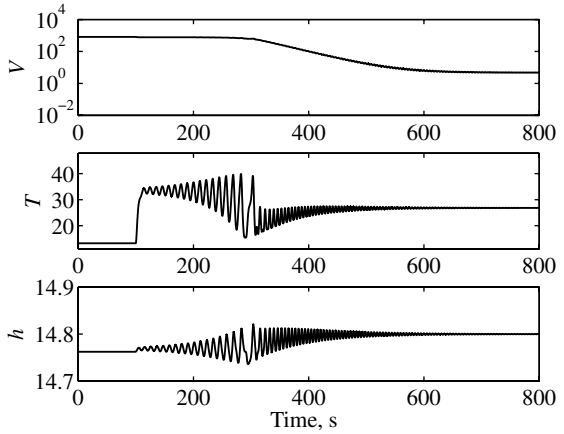

Fig. 11 Lyapunov function V, kinetic energy T (J), and total angular momentum magnitude h (N · m · s) for flat-spin recovery with mass-property and wheel-alignment errors.

the proposed control law is not sensitive to typical errors encountered in practice.

V. Conclusions

The Lyapunov control law presented in this paper provides a practical technique for stabilizing prolate spin on small spacecraft. The control hardware is compatible with low-cost spacecraft, requiring only one reaction wheel with an integral tachometer and one rate gyro aligned with the wheel spin axis. The control law can be a simple linear proportional feedback of sensed angular velocity and relative wheel rate to reaction-wheel torque, which could be implemented in rugged analog electronics or in a low-cost microcontroller. Wheel mounting is only constrained to be transverse to the desired spin axis and not aligned with the major principal axis for the theoretical results, promoting the idea of a modular, self-contained, spin-stabilization assembly (reaction wheel and rate gyro) that could be added to a spacecraft instead of ballast mass or embarking on a major redesign to obtain oblate mass properties. All that is needed from the spacecraft is electrical power, enabling long-lived operational spin about a minor principal axis.

Analysis of this control law revealed that conventional global asymptotic stability is not possible with this single-wheel approach, which can be traced to underactuation. Despite the relatively weak semidefinite Lyapunov functions and derivatives that result, a strong LaSalle invariance result was derived, leading to the conclusion that prolate spin is *essentially globally asymptotically stable*. That is, there are only four other spin equilibria, and conditions were given so that these are always unstable. The stable manifolds entering these equilibria are thin (sets measure zero in the angular momentum constraint manifold), hence the state cannot remain near these equilibria in practice, due to measurement noise and numerical errors in the control law. In particular, this control law provides guaranteed recovery from arbitrary launch-vehicle tipoff conditions, including flat spin (major-axis spin).

The control law contains two free parameters that can be adjusted to obtain variations in nutation-damping rates and corresponding wheel torque and power requirements. A preliminary empirical study [50] investigated optimal settling times for this control approach. More generally, a family of control laws is exhibited in which any odd function can be applied to the linear feedback. Variations of the control law within this family may enable more efficient use of small reaction wheels with limited power and torque. The simulation examples presented here show that the effect of the Lyapunov control law can be designed to produce a minor modification to the rigid-body spacecraft dynamics, producing qualitatively similar nutation behavior that is well-understood, except that stability properties of oblate and prolate spin are interchanged. This control law requires only a subtle change in the spacecraft kinetic energy over time. In turn, the proposed control law requires correspondingly small electrical-energy requirements and appears to be robust to uncertainty in spacecraft mass properties and wheel misalignment.

Appendix A: Passive Equilibrium Stability

Suppose that the locked-rotor mass properties satisfy $\bar{A} > \bar{B} > \bar{C}$ with principal axes $(\bar{\mathbf{1}}, \bar{\mathbf{2}}, \bar{\mathbf{3}})$. Consider deviations from equilibrium spin about the $\bar{\mathbf{2}}$ (intermediate) axis in the form $\boldsymbol{\omega}_b = \alpha\bar{\mathbf{1}} + \beta\bar{\mathbf{2}}$. When constrained to the manifold of constant angular momentum magnitude h_o with $u = 0$,

$$h_o^2 = \boldsymbol{\omega}_b \cdot \left(\mathbf{I}_b^{o_s} + \mathbf{I}_w^{o_s}\right) \cdot \boldsymbol{\omega}_b = \alpha^2\bar{A}^2 + \beta^2\bar{B}^2 \tag{A1}$$

The corresponding kinetic energy is then

$$\begin{aligned} T &= \alpha^2\bar{A} + \beta^2\bar{B} = \alpha^2\bar{A} + \left(h_o^2 - \alpha^2\bar{A}^2\right)/\bar{B} \\ &= h_o^2/\bar{B} + \alpha^2\bar{A}(\bar{B} - \bar{A})/\bar{B} \end{aligned} \tag{A2}$$

The first term on the right is the kinetic energy T_2 for $\bar{\mathbf{2}}$-axis equilibrium spin, and the second term is negative for all $\alpha \neq 0$. Thus, there are states in every neighborhood of this equilibrium within the angular momentum manifold that have $T < T_2$.

Because $\dot{T} \leq 0$, motion beginning on any such initial state will converge to one of the *other* equilibrium spins (as shown in Sec. III) with corresponding $T = T_i$, where $T_i < T_2$. Thus, equilibrium spin about the $\bar{\mathbf{2}}$ axis (intermediate axis) is Lyapunov-unstable.

Similarly, for equilibrium spin about the $\bar{\mathbf{3}}$ axis, $\boldsymbol{\omega}_b$ in the form $\alpha\bar{\mathbf{1}} + \eta\bar{\mathbf{3}}$ with $u = 0$ results in $T = h_o^2/\bar{C} + \alpha^2\bar{A}(\bar{C} - \bar{A})/\bar{C}$, showing that there are states in every neighborhood of $\bar{\mathbf{3}}$-axis equilibrium spin within the angular momentum manifold that have smaller kinetic energy, and this equilibrium (minor-axis spin) is also Lyapunov-unstable.

When $\bar{B} > \bar{A} > \bar{C}$, note that the preceding argument for $\bar{\mathbf{3}}$-axis (minor-axis) spin holds. For $\bar{\mathbf{1}}$-axis spin (now the intermediate axis), write Eq. (A2) in the form $T = h_o^2/\bar{A} + \beta^2\bar{B}(\bar{A} - \bar{B})/\bar{A}$ to show instability.

Appendix B: Lyapunov Derivative

The time derivative of the scalar Eq. (15) is given by

$$\begin{aligned} \dot{V} = \frac{{}^G\mathrm{d}}{\mathrm{d}t}V = &2[(\mathbf{I}_B - \mathbf{I}_C)\cdot\boldsymbol{\omega}_b + K\Omega\hat{\mathbf{a}}]\cdot\tfrac{{}^G\mathrm{d}}{\mathrm{d}t}(\mathbf{M}\cdot[(\mathbf{I}_B - \mathbf{I}_C)\cdot\boldsymbol{\omega}_b \\ &+ K\Omega\hat{\mathbf{a}}]) + 2K^2\Gamma^2\Omega\dot{\Omega} \end{aligned} \tag{B1}$$

where G is any frame. Because $\mathbf{M}$, $\mathbf{I}_B$, and $\mathbf{I}_C$ are fixed in the body frame F, we use the F frame derivative to obtain

$$\begin{aligned} \dot{V} = 2[(\mathbf{I}_B - \mathbf{I}_C)\cdot\boldsymbol{\omega}_b + K\Omega\hat{\mathbf{a}}]\cdot\Bigg(\mathbf{M}\cdot\Bigg[(\mathbf{I}_B - \mathbf{I}_C)\cdot\frac{{}^F\mathrm{d}}{\mathrm{d}t}\boldsymbol{\omega}_b \\ + K\dot{\Omega}\,\hat{\mathbf{a}}\Bigg]\Bigg) + 2K^2\Gamma^2\Omega\dot{\Omega} \end{aligned} \tag{B2}$$

Substituting the spacecraft dynamics [Eq. (9)] results in

$$\begin{aligned} \dot{V} = &-2[(\mathbf{I}_B - \mathbf{I}_C)\cdot\boldsymbol{\omega}_b + K\Omega\hat{\mathbf{a}}]\cdot\mathbf{M}\cdot(\mathbf{I}_B - \mathbf{I}_C)\cdot\mathbf{I}_B^{-1} \\ &\cdot[\boldsymbol{\omega}_b\times(\mathbf{I}_B\cdot\boldsymbol{\omega}_b + K\Omega\hat{\mathbf{a}}) + K\dot{\Omega}\,\hat{\mathbf{a}}] + 2K\dot{\Omega}[(\mathbf{I}_B - \mathbf{I}_C) \\ &\cdot\boldsymbol{\omega}_b + K\Omega\hat{\mathbf{a}}]\cdot\mathbf{M}\cdot\hat{\mathbf{a}} + 2K^2\Gamma^2\Omega\dot{\Omega} \end{aligned} \tag{B3}$$

The form of $\mathbf{M}$ given in Eq. (17) produces

$$\mathbf{M}\cdot(\mathbf{I}_B - \mathbf{I}_C)\cdot\mathbf{I}_B^{-1} = \delta(\mathbf{I} - \hat{\mathbf{3}}\,\hat{\mathbf{3}}) \tag{B4}$$

where δ is defined in Eq. (19); thus,

$$\dot{V} = -2\delta[(\mathbf{I}_B - \mathbf{I}_C)\cdot\boldsymbol{\omega}_b + K\Omega\hat{\mathbf{a}}]\cdot[\boldsymbol{\omega}_b \times (\mathbf{I}_B\cdot\boldsymbol{\omega}_b + K\Omega\hat{\mathbf{a}}) + K\dot{\Omega}\,\hat{\mathbf{a}}] + 2\delta[(\mathbf{I}_B - \mathbf{I}_C)\cdot\boldsymbol{\omega}_b + K\Omega\hat{\mathbf{a}}]\cdot\hat{\mathbf{3}}\,\hat{\mathbf{3}}\cdot[\boldsymbol{\omega}_b \times (\mathbf{I}_B\cdot\boldsymbol{\omega}_b + K\Omega\hat{\mathbf{a}}) + K\dot{\Omega}\,\hat{\mathbf{a}}] + 2K\dot{\Omega}[(\mathbf{I}_B - \mathbf{I}_C)\cdot\boldsymbol{\omega}_b + K\Omega\hat{\mathbf{a}}]\cdot\mathbf{M}\cdot\hat{\mathbf{a}} + 2K^2\Gamma^2\Omega\dot{\Omega} \tag{B5}$$

Write the first term of Eq. (B5) in the form

$$-2\delta[\mathbf{I}_B\cdot\boldsymbol{\omega}_b + K\Omega\hat{\mathbf{a}}]\cdot[\boldsymbol{\omega}_b \times (\mathbf{I}_B\cdot\boldsymbol{\omega}_b + K\Omega\hat{\mathbf{a}})] + 2\delta[\mathbf{I}_C\cdot\boldsymbol{\omega}_b]\cdot[\boldsymbol{\omega}_b \times (\mathbf{I}_B\cdot\boldsymbol{\omega}_b + K\Omega\hat{\mathbf{a}})] - 2K\dot{\Omega}\delta[(\mathbf{I}_B - \mathbf{I}_C)\cdot\boldsymbol{\omega}_b + K\Omega\hat{\mathbf{a}}]\cdot\hat{\mathbf{a}} \tag{B6}$$

The vector identity $\mathbf{x}\cdot(\mathbf{x}\times\mathbf{y}) = 0$ shows that the first term in Eq. (B6) is zero. Similarly, because $\mathbf{I}_C\cdot\boldsymbol{\omega}_b = C\boldsymbol{\omega}_b$, the second term in Eq. (B6) is also zero. The second term in Eq. (B5) is zero because $\mathbf{I}_B - \mathbf{I}_C$ is a projection onto the $\hat{\mathbf{1}}$–$\hat{\mathbf{2}}$ plane, and $\hat{\mathbf{a}}$ is restricted to that plane. Combining the surviving third and fourth terms of Eq. (B5) and the third term of Eq. (B6), we obtain

$$\dot{V} = 2K\dot{\Omega}\{[(\mathbf{I}_B - \mathbf{I}_C)\cdot\boldsymbol{\omega}_b + K\Omega\hat{\mathbf{a}}]\cdot(\mathbf{M} - \delta\mathbf{I})\cdot\hat{\mathbf{a}} + K\Gamma^2\Omega\} \tag{B7}$$

Using the expressions in Eqs. (3), (16), (17), and (B7) simplifies to Eqs. (18) and (19).

Appendix C: Invariant Set *S* Properties

From Eq. (21), we have the set P (where $\dot{V} = 0$) defined by the linear constraint on $\Re^3 \times \Re$:

$$0 = (C\delta + \gamma)\boldsymbol{\omega}_b\cdot\hat{\mathbf{a}} + \gamma u = C\delta\boldsymbol{\omega}_b\cdot\hat{\mathbf{a}} + \gamma\Omega \tag{C1}$$

This defines P as a three-dimensional subspace of $\Re^4$ spanned by

$$\mathbf{v}_1 = (\gamma\hat{\mathbf{a}}, -C\delta), \qquad \mathbf{v}_2 = (\hat{\mathbf{b}}, 0), \qquad \mathbf{v}_3 = (\hat{\mathbf{3}}, 0) \tag{C2}$$

where $\hat{\mathbf{b}} = \hat{\mathbf{3}}\times\hat{\mathbf{a}}$, so that every element of P has the form

$$(\boldsymbol{\omega}_b, \Omega) = \sigma_1\mathbf{v}_1 + \sigma_2\mathbf{v}_2 + \sigma_3\mathbf{v}_3 = (\sigma_1\gamma\hat{\mathbf{a}} + \sigma_2\hat{\mathbf{b}} + \sigma_3\hat{\mathbf{3}}, -\sigma_1 C\delta) \tag{C3}$$

for some $\sigma_i \in \Re$. Substituting Eq. (C3) into the closed-loop dynamics [Eqs. (9), (10), and (20)] produces a vector field on P. Generally, this vector field does not lie in P, hence some initial states in P will not remain in P. To be invariant, $S \subset P$ contains only those states for which the closed-loop vector field lies in P. Therefore every element of S has a (body frame) time derivative that can also be represented in σ_i coordinates, producing a set of differential equations in the σ_i. Solutions to this set of ordinary differential equations (ODEs) are the only closed-loop state trajectories that remain in P. The largest invariant set S therefore consists of all solutions to these ODEs.

First, note that using Eq. (C1) in Eq. (20) produces $e = Nu$, and in Eq. (10) this implies that $\dot{\Omega} = 0$. Taking the body-frame time derivative of Eq. (C3), we immediately see that $\dot{\sigma}_1 = 0$. Writing $\boldsymbol{\omega}_b = \sigma_1\gamma\hat{\mathbf{a}} + \sigma_2\hat{\mathbf{b}} + \sigma_3\hat{\mathbf{3}}$ and $\dot{\boldsymbol{\omega}}_b = \dot{\sigma}_1\gamma\hat{\mathbf{a}} + \dot{\sigma}_2\hat{\mathbf{b}} + \dot{\sigma}_3\hat{\mathbf{3}}$ in coordinates of the body $(\hat{\mathbf{1}}, \hat{\mathbf{2}}, \hat{\mathbf{3}})$ frame and substituting into Eq. (9) results in

$$\begin{aligned}
A\dot{\sigma}_2\sin\theta &= C\sigma_3(\sigma_1\gamma\sin\theta + \sigma_2\cos\theta) - \sigma_3[\sigma_1(B\gamma - KC\delta)\sin\theta + B\sigma_2\cos\theta]\\
B\dot{\sigma}_2\cos\theta &= C\sigma_3(\sigma_1\gamma\cos\theta - \sigma_2\sin\theta) - \sigma_3[\sigma_1(A\gamma - KC\delta)\cos\theta - A\sigma_2\sin\theta]\\
C\dot{\sigma}_3 &= -(\sigma_1\gamma\cos\theta - \sigma_2\sin\theta)[\sigma_1(B\gamma - KC\delta)\sin\theta + B\sigma_2\cos\theta]\\
&\quad + (\sigma_1\gamma\sin\theta + \sigma_2\cos\theta)[\sigma_1(A\gamma - KC\delta)\cos\theta - A\sigma_2\sin\theta]
\end{aligned} \tag{C4}$$

Combining the first two equations results in the constraint

$$\begin{aligned}
&BC\sigma_3\cos\theta(\sigma_1\gamma\sin\theta + \sigma_2\cos\theta)\\
&\quad - B\sigma_3\cos\theta[\sigma_1(B\gamma - KC\delta)\sin\theta + B\sigma_2\cos\theta]\\
&\quad = AC\sigma_3\sin\theta(\sigma_1\gamma\cos\theta - \sigma_2\sin\theta)\\
&\quad - A\sigma_3\sin\theta[\sigma_1(A\gamma - KC\delta)\cos\theta - A\sigma_2\sin\theta]
\end{aligned} \tag{C5}$$

Consider separately the cases in which $\sigma_3 \equiv 0$ and $\sigma_3 \not\equiv 0$. When $\sigma_3 \equiv 0$, Eq. (C5) is satisfied and the corresponding solution to Eq. (C4) must have $\dot{\sigma}_3 = 0$. Note that $\dot{\sigma}_2$ is also zero. This results in a constraint between equilibrium values σ_1 and σ_2 in the form

$$(\sigma_1\gamma)^2(B - A)\cos\theta\sin\theta - (\sigma_1\gamma)\sigma_2[-KC\delta + (B - A)(\sin^2\theta - \cos^2\theta)] - \sigma_2^2(B - A)\cos\theta\sin\theta = 0 \tag{C6}$$

If $A = B$, this requires $\sigma_1\sigma_2 = 0$, because $KC\delta\gamma \neq 0$. This produces two solutions for σ_2, satisfying the momentum constraint when $\sigma_1 = 0$ (spin about $\hat{\mathbf{b}}$ with no wheel spin Ω), and two solutions for σ_1 when $\sigma_2 = 0$ (spin about $\hat{\mathbf{a}}$ with a proportional wheel spin Ω). When $A \neq B$, consider separately the cases when $\sin\theta = 0$ and when $\cos\theta = 0$. This results in the constraints

$$\sigma_1\sigma_2\gamma(B - A + KC\delta) = 0, \qquad \sigma_1\sigma_2\gamma(A - B + KC\delta) = 0 \tag{C7}$$

respectively. If we specify (Assumption 5) that the wheel $\hat{\mathbf{a}}$ axis is not aligned with the body major axis, we have $B > A$ when $\sin\theta = 0$ and $A > B$ when $\cos\theta = 0$. Because $\delta > 0$, the preceding cases then reduce to $\sigma_1\sigma_2 = 0$ as before.

In the more general case in which $(A - B)\sin\theta\cos\theta \neq 0$, Eq. (C6) becomes

$$(\sigma_1\gamma)^2 - c_1(\sigma_1\gamma)\sigma_2 - \sigma_2^2 = 0 \tag{C8}$$

where

$$c_1 = \frac{KC\delta/[\gamma(A - B)] + \sin^2\theta - \cos^2\theta}{\cos\theta\sin\theta} \tag{C9}$$

From the quadratic formula, σ_1 and σ_2 satisfy the two linear relations:

$$\gamma\sigma_1 = c_2\sigma_2, \qquad c_2 = c_1/2 \pm \sqrt{c_1^2/4 + 1} \tag{C10}$$

Note that c_2 is finite and nonzero here, so that equilibrium lines do not align with the wheel axis $\hat{\mathbf{a}}$ or the transverse axis $\hat{\mathbf{b}}$. It is desirable to locate the wheel so that these equilibrium lines also do not coincide with the locked-rotor principal axes $\mathbf{I}_b^{o_s} + \mathbf{I}_w^{o_s}$, promoting flat-spin recovery, as discussed in Sec. IV. Along with $\sigma_3 = 0$ and the constant total momentum, this again produces a set of four distinct points in P that are invariant. These are undesired equilibria, because they do not result in spin about the $\hat{\mathbf{3}}$ axis.

Returning to Eq. (C5), suppose $\sigma_3 \not\equiv 0$. At any time that $\sigma_3 \neq 0$, we obtain a linear relation between σ_1 and σ_2 in the form

$$\sigma_2 = m\sigma_1 \tag{C11}$$

where

$$m = \frac{(B - A)\cos\theta\sin\theta[(C - A - B)\gamma + KC\delta]}{B(B - C)\cos^2\theta + A(A - C)\sin^2\theta} \tag{C12}$$

From the previous finding that $\dot{\sigma}_1 = 0$, this implies that $\dot{\sigma}_2 = 0$. Using Eq. (C11) in Eq. (C4) produces two constraints:

$$\begin{aligned}
\sigma_1[(B - C)(\gamma\sin\theta + m\cos\theta) - KC\delta\sin\theta] &= 0\\
\sigma_1[(A - C)(\gamma\cos\theta - m\sin\theta) - KC\delta\cos\theta] &= 0
\end{aligned} \tag{C13}$$

For the coefficients of σ_1 to be zero in both of these, we need γ to satisfy, respectively

$$\gamma = \frac{KC\delta}{B-C} - m\frac{\cos\theta}{\sin\theta}, \qquad \gamma = \frac{KC\delta}{A-C} + m\frac{\sin\theta}{\cos\theta} \tag{C14}$$

Equating these and solving for m yields

$$m = KC(A-B)\cos\theta\sin\theta \tag{C15}$$

If $(A-B)\cos\theta\sin\theta \neq 0$, Eqs. (C12) and (C15) together with Eq. (19) imply that $\Gamma = 0$. Thus, both coefficients of σ_1 in Eq. (C13) cannot be zero when $\Gamma \neq 0$, implying that $\sigma_1 = 0$, and from Eq. (C11), $\sigma_2 = 0$. Using this in Eq. (C4) results in $\dot{\sigma}_3 = 0$. Because $\sigma_3 \neq 0$, this represents the desired equilibrium spin about the $\hat{\mathbf{3}}$ axis. The two values of spin rate $\pm\omega_o$ will be determined by the angular momentum constraint. If $A = B$, then $m = 0$, hence $\sigma_2 = 0$, and Eq. (C14) yields $\Gamma = 0$ as before. If $A \neq B$ but $\cos\theta\sin\theta = 0$, then Eq. (C14) cannot both be satisfied (for any Γ), and both $\sigma_1 = 0$ and $\sigma_2 = 0$, resulting in the same two $\hat{\mathbf{3}}$-axis equilibria as before.

Together with the four undesired equilibria found earlier, these two desired equilibria constitute the largest invariant set S in P. Because $\dot{V} \leq 0$ in the entire state space, the LaSalle invariance principle [46] implies that beginning at any initial state, the spacecraft angular velocities converge to one of these six equilibria in the invariant set S. This is a particularly strong result, given that both the Lyapunov function and its derivative are only semidefinite functions in the neighborhood of these equilibria. Specifically, this result implies that all state trajectories that begin away from an equilibrium result in a strict decrease in V; otherwise, S must contain more than six isolated points. We will use this in Appendix D to show instability of the undesired equilibria and asymptotic stability of the desired minor-axis spin.

Appendix D: Stability of Equilibrium Points in S

We show that level sets of V passing through undesired equilibria U_i are distinct from the constant angular momentum magnitude constraint. This is combined with the results of Appendix C, which show that $\dot{V}$ is strictly decreasing for state trajectories originating in neighborhoods of the U_i, to show that these equilibria are unstable. Methods such as Chetayev's instability theorems [46,57] require assumptions (such as negative definite $\dot{V}$) that are not satisfied here.

To begin, let $\mathbf{h}$ at the equilibrium $U_i = (\boldsymbol{\omega}_{bi}, \Omega_i)$ be designated by

$$\mathbf{h}_i = \mathbf{I}_B \cdot \boldsymbol{\omega}_{bi} + K\Omega_i\hat{\mathbf{a}} \tag{D1}$$

and let $h_i^2 = \mathbf{h}_i \cdot \mathbf{h}_i$. Note that these undesired equilibria have a zero $\hat{\mathbf{3}}$-axis component for $\mathbf{h}_i$, because this is true for $\boldsymbol{\omega}_{bi}$ from Appendix C, and $\hat{\mathbf{a}}$ lies in the $\hat{\mathbf{1}}$–$\hat{\mathbf{2}}$ plane. Because $h_i > 0$, $\mathbf{h}_i \cdot \hat{\mathbf{1}}$ and $\mathbf{h}_i \cdot \hat{\mathbf{2}}$ cannot both be zero.

Suppose $\mathbf{h}_i \cdot \hat{\mathbf{1}} \neq 0$, and consider states $(\boldsymbol{\omega}_b, \Omega)$ in the neighborhood of this equilibrium given by

$$\boldsymbol{\omega}_b = \boldsymbol{\omega}_{bi} + \alpha\hat{\mathbf{1}} + \beta\hat{\mathbf{3}}, \qquad \Omega = \Omega_i \tag{D2}$$

This results in

$$h^2 = h_i^2 + 2\mathbf{h}_i \cdot (A\alpha\hat{\mathbf{1}} + C\beta\hat{\mathbf{3}}) + A^2\alpha^2 + C^2\beta^2 \tag{D3}$$

so that motion on the constant momentum constraint (which has the same momentum magnitude as at the equilibrium) requires that α and β are related by

$$0 = \alpha[2A(\mathbf{h}_i \cdot \hat{\mathbf{1}})] + \beta[2C(\mathbf{h}_i \cdot \hat{\mathbf{3}})] + \alpha^2[A^2] + \beta^2[C^2] \tag{D4}$$

where $(\mathbf{h}_i \cdot \hat{\mathbf{3}}) = 0$.

Using Eq. (D2) in V from Eq. (15), the change from the equilibrium value $V - V_i$ is found to be

$$\Delta V = (A-C)(B-C)[2\alpha A(\mathbf{h}_i - \mathbf{I}_c \cdot \boldsymbol{\omega}_{bi}) \cdot \hat{\mathbf{1}} + \alpha^2 A(A-C)] \tag{D5}$$

Now note that $\mathbf{h}_i - \mathbf{I}_c \cdot \boldsymbol{\omega}_{bi}$ is colinear with $\mathbf{h}_i$ at an equilibrium; because $\dot{\boldsymbol{\omega}}_b$ and $\dot{\Omega}$ are zero and Eq. (9) requires that $\boldsymbol{\omega}_{bi} \times \mathbf{h}_i = 0$, then $\boldsymbol{\omega}_{bi}$ and $\mathbf{h}_i$ are colinear, as is $\mathbf{I}_c \cdot \boldsymbol{\omega}_{bi} = C\boldsymbol{\omega}_{bi}$. Define the scalar r_i by

$$\mathbf{h}_i - \mathbf{I}_c \cdot \boldsymbol{\omega}_{bi} = r_i\mathbf{h}_i \tag{D6}$$

Replacing the term in Eq. (D5) linear in α by the corresponding momentum constraint (D4) term yields

$$\Delta V = (A-C)(B-C)(\alpha^2A^2\left(1 - r_i - \frac{C}{A}\right) - \beta^2C^2r_i) \tag{D7}$$

It is shown next that there is a Γ large enough so that $r_i > 0$. Hence, ΔV satisfies

$$\Delta V \leq \alpha^2(A-C)(B-C)\left[A^2\left(1 - \frac{C}{A}\right) - \frac{\beta^2}{\alpha^2}C^2r_i\right] \tag{D8}$$

From Eq. (D4), we find that

$$\frac{\beta^2}{\alpha^2} = -\frac{A^2}{C^2} - \frac{2A(\mathbf{h}_i \cdot \hat{\mathbf{1}})}{\alpha C^2} \tag{D9}$$

Hence, Eq. (D4) admits nonzero solutions for α and β and β^2/α^2 is unbounded on every neighborhood of $(0,0)$ because $\mathbf{h}_i \cdot \hat{\mathbf{1}} \neq 0$. Then every neighborhood of the equilibrium U_i on the momentum constraint has points for which $\Delta V < 0$.

If $\mathbf{h}_i \cdot \hat{\mathbf{1}} = 0$, then $\mathbf{h}_i \cdot \hat{\mathbf{2}} \neq 0$, so consider the deviation similar to Eq. (D2):

$$\boldsymbol{\omega}_b = \boldsymbol{\omega}_{bi} + \alpha\hat{\mathbf{2}} + \beta\hat{\mathbf{3}}, \qquad \Omega = \Omega_i \tag{D10}$$

When $r_i > 0$, this results in

$$\Delta V \leq \alpha^2(A-C)(B-C)\left[B^2\left(1 - \frac{C}{B}\right) - \frac{\beta^2}{\alpha^2}C^2r_i\right] \tag{D11}$$

and

$$\frac{\beta^2}{\alpha^2} = -\frac{B^2}{C^2} - \frac{2B(\mathbf{h}_i \cdot \hat{\mathbf{2}})}{\alpha C^2} \tag{D12}$$

which is unbounded on every neighborhood of $\alpha = 0$ and $\beta = 0$ because $\mathbf{h}_i \cdot \hat{\mathbf{2}} \neq 0$, and $\Delta V < 0$ on every neighborhood of U_i.

We now show that $r_i > 0$, as claimed earlier. Using Eqs. (C3) and (C10) in Eq. (D6) and expanding the $\hat{\mathbf{1}}$ component, the solution for r_i is found to be

$$r_i = 1 - \left(\frac{A}{C} - W_i\right)^{-1} \tag{D13}$$

where

$$W_i = \left(\frac{K\delta}{\gamma}\right)\left(1 - \frac{\tan\theta}{c_{2i}}\right)^{-1}$$

Note that $r_i > 0$ when $W_i < (A-C)/C$. Also, $\tan\theta/c_{2i} \leq 0$ produces $W_i \leq K\delta/\gamma$. Now

$$\frac{K\delta}{\gamma} \leq \frac{A-C}{C} \tag{D14}$$

expands to

$$C(B-A)\sin^2\theta \leq \Gamma^2 \tag{D15}$$

which is satisfied by choice of a large-enough control parameter Γ.

Evaluating the $\hat{\mathbf{2}}$ component of Eq. (D6) provides an alternate expression for r_i:

$$r_i = 1 - \left(\frac{B}{C} - Q_i\right)^{-1} \tag{D16}$$

where

$$Q_i = \left(\frac{K\delta}{\gamma}\right)\left(1 + \frac{\cot\theta}{c_{2i}}\right)^{-1}$$

Here, $r_i > 0$ when $Q_i < (B - C)/C$. When $\tan\theta/c_{2i} > 0$, we have $\cot\theta/c_{2i} > 0$ and this produces $Q_i < K\delta/\gamma$. Now

$$\frac{K\delta}{\gamma} < \frac{B - C}{C} \tag{D17}$$

expands to

$$C(A - B)\cos^2\theta < \Gamma^2 \tag{D18}$$

Both Eqs. (D15) and (D18) are satisfied by choosing $\Gamma^2 > C|A - B|$, and we have $r_i > 0$ for all values of $\tan\theta/c_{2i}$.

Thus, for any $A > C, B > C$, and any θ, $\Delta V < 0$ in a neighborhood of any of the undesired equilibria, provided that Γ is chosen to be large enough in the control law.

Instability of the undesired equilibria is now straightforward. For any neighborhood of U_i in the constant momentum manifold, there are initial conditions $\boldsymbol{\omega}_{bo}$ and Ω_o that have Lyapunov function values V_o strictly less than the value V_i at U_i. By the results of Appendix C, the system state converges to one of the *other* undesired equilibria U_j, where $V_j \leq V_o < V_i$, or to one of the desired equilibria that has $V = 0$. Hence, the undesired equilibrium U_i is unstable. Because U_i was arbitrary, all four undesired equilibria are unstable.

If A_o designates the set for which V is less than the smallest of the values of V_i among the four undesired equilibria, then the set A_o is a basin of attraction for the two desired equilibria, because no other invariant sets lie in the intersection of P and A_o. Initial states in A_o converge to a desired equilibrium, and V converges to zero. The desired equilibria are therefore asymptotically stable.

Note that the preceding results do not say that all initial conditions near an undesired equilibrium are repelled. The center manifold theorem [58] shows that these unstable undesired equilibria may have stable manifolds, attracting some trajectories to themselves. However, these stable manifolds must be thin; the evolution of angular velocities in the neighborhood of these equilibria are constrained to lie on the constant angular momentum cylinder $H \subset \Re^4$. The state evolution on this three-dimensional manifold H about an undesired equilibrium is not stable, as shown earlier. Therefore, there is an unstable submanifold of H of the dimension of at least one about each U_i. Any stable manifold about U_i therefore has dimension of, at most, two. Initial states exactly on this submanifold would converge to the corresponding U_i, but any disturbance from this thin set would result in motion away from the undesired equilibrium. These stable manifolds have a measure of zero in the three-dimensional angular momentum manifold H, hence the desired equilibria are *essentially* globally asymptotically stable (i.e., except for a set of initial conditions of measure zero).

Indeed, a spot check of the eigenvalues of the linearized state matrix about these four equilibria for specific values of mass properties, feedback gain κ, and angular momentum (corresponding to the first simulation example in Sec. IV) shows that negative real-part eigenvalues (hence stable manifolds) do exist for all four of these undesired equilibria: the stable manifolds are one-dimensional for two U_i and two-dimensional for the other two U_i. That is, except for initial conditions on a line into two undesired equilibria and on a thin two-dimensional sheet at the other two undesired equilibrium points, all initial states result in convergence to one of the two desired equilibria.

Acknowledgments

This work was supported by the Center for Space Construction at the University of Colorado under NASA grants NAGW 1388, NGT 10033, NGT 538, and NAG5-4100. The authors wish to thank the anonymous reviewers for their detailed critiques and helpful comments.

References

[1] Likins, P., "Attitude Stability Criteria for Dual Spin Spacecraft," *Journal of Spacecraft and Rockets*, Vol. 40, No. 6, 2003, pp. 946–951.

[2] Hablani, H., "Interplanetary Spacecraft Controllers Using Thrusters," *Journal of Guidance, Control, and Dynamics*, Vol. 21, No. 4, 1998, pp. 542–550.

[3] Solomon, S., Bailey, S., Barth, C., Davis, R., Donnelly, J., and Holden, T., "The SNOE Spacecraft: Integration, Test, Launch, Operation, and On-Orbit Performance," *Proceedings of the 12th AIAA/USU Conference on Small Satellites*, Utah State Univ., Logan, UT, 1998.

[4] fDevey, W., Field, C., and Flook, L., "An Active Nutation Control System for Spin Stabilized Satellites," *Automatica*, Vol. 13, No. 2, 1977, pp. l61–172.

[5] Bracewell, R., and Garriott, O. K., "Rotation of Artificial Earth Satellites," *Nature*, Vol. 182, No. 4638, 1958, pp. 760–762.

[6] Reiter, G., and Thomson, W., "Rotational Motion of Passive Space Vehicles," *Torques and Attitude Sensing in Earth Satellites*, edited by S. Singer, Academic Press, New York, 1964.

[7] Garg, S., Furumoto, N., and Vanyo, J., "Spacecraft Nutational Instability Prediction by Energy-Dissipation Measurements," *Journal of of Guidance, Control, and Dynamics*, Vol. 9, No. 3, 1986, pp. 357–362.

[8] Bialke, B., "High Fidelity Mathematical Modeling of Reaction Wheel Performance," 21st AAS Conference on Guidance and Control, Breckenridge, CO, American Astronautical Society Paper 98-063, Feb. 1998.

[9] Fowell, R. A., Milford, R. I., and Yocum, J. F., "Spacecraft Spin Stabilization Using a Transverse Wheel for Any Inertia Ratio," *Journal of Guidance, Control, and Dynamics*, Vol. 22, No. 6, Dec. 1999, pp. 768–775.

[10] White, J. E., and Robinett, R. D., III, "Principal Axis Misalignment Control for Deconing of Spinning Spacecraft," *Journal of Guidance, Control and Dynamics*, Vol. 17, No. 4, 1994, pp. 823–830.

[11] Bloch, A. M., Chang, D. E., Leonard, N. E., Marsden, J. E., and Woolsey, C., "Asymptotic Stabilization of Euler-Poincare Mechanical Systems," *Lagrangian and Hamiltonian Methods for Nonlinear Control*, Elsevier, Oxford, England, U.K., 2000, pp. 51–56.

[12] Bloch, A. M., Leonard, N. E., and Marsden, J. E., "Controlled Lagrangians and the Stabilization of Euler-Poincare Mechanical Systems," *International Journal of Robust and Nonlinear Control*, Vol. 11, No. 3, 2001, pp. 191–214.

[13] Zhao, R., and Posbergh, T. A., "Stabilization of a Rotating Rigid Body by the Energy Momentum Method," *Proceedings of the 31st IEEE Conference on Decision and Control* , Inst. of Electrical and Electronics Engineers, New York, Dec. 1992, pp. 1583–1588.

[14] Crouch, P. E., "Spacecraft Attitude Control and Stabilization: Applications of Geometric Control Theory to Rigid Body Models," *IEEE Transactions on Automatic Control*, Vol. AC-29, No. 4, Apr. 1984, pp. 321–331.

[15] Byrnes, C., and Isidori, A., "On the Attitude Stabilization of Rigid Spacecraft," *Automatica*, Vol. 27, No. 1, 1991, pp. 87–95.

[16] Krishnan, H., Reyhanoglu, M., and McClamroch, H., "Attitude Stabilization of a Rigid Spacecraft Using Gas Jet Actuators Operating in a Failure Mode," *Proceedings of the 31st IEEE Conference on Decision and Control* , Inst. of Electrical and Electronics Engineers, New York, Dec. 1992, pp. 1612–1617.

[17] Robinett, R. D., and Parker, G. G., "Least Squares Sliding Mode Control Tracking of Spacecraft Large Angle Maneuvers," *Journal of the Astronautical Sciences*, Vol. 45, No. 4, 1997, pp. 433–450.

[18] Schaub, H., Vadali, S. R., and Junkins, J. L., "Feedback Control Law for Variable Speed Control Moment Gyros," *Journal of the Astronautical Sciences*, Vol. 46, No. 3, 1998, pp. 307–328.

[19] Tsiotras, P., and Luo, J., "Reduced Effort Control Laws for Underactuated Rigid Spacecraft," *Journal of Guidance, Control, and Dynamics*, Vol. 20, No. 6, 1997, pp. 1089–1095.

[20] Tsiotras, P., and Schleicher, A., "Detumbling and Partial Attitude Stabilization of a Rigid Spacecraft Under Actuator Failure," AIAA Guidance, Navigation and Control Conference, Denver, CO, AIAA Paper 2000-4044, Aug. 2000.

[21] Aeyels, D., "Stabilization by Smooth Feedback of the Angular Velocity of a Rigid Body," *Systems and Control Letters*, Vol. 5, 1985, pp. 59–63.

[22] Aeyels, D., and Szafranski, M., "Comments on the Stabilizability of the Angular Velocity of a Rigid Body," *Systems and Control Letters*, Vol. 10, No. 1, 1988, pp. 35–39.

[23] Outbib, R., and Sallet, G., "Stabilizability of the Angular Velocity of a Rigid Body," *Systems and Control Letters*, Vol. 18, No. 2, 1992, pp. 93–98.
[24] Wan, C.-J., and Bernstein, D. S., "A Family of Optimal Nonlinear Feedback Controllers That Globally Stabilize Angular Velocity," *Proceedings of the 31st IEEE Conference on Decision and Control* , Inst. of Electrical and Electronics Engineers, New York, 1992, pp. 1143–1148.
[25] Wan, C.-J., and Bernstein, D. S., "Rotational Stabilization of a Rigid Body Using Two Torque Actuators," *Proceedings of the 32nd IEEE Conference on Decision and Control* , Inst. of Electrical and Electronics Engineers, New York, 1993, pp. 3111–3116.
[26] Coverstone-Carrol, V., "Detumbling and Reorienting Underactuated Rigid Spacecraft," *Journal of Guidance, Control, and Dynamics*, Vol. 19, No. 3, 1996, pp. 708–710.
[27] Robinett, R. D., Parker, G. G., Schaub, H., and Junkins, J. L., "Lyapunov Optimal Saturated Control for Nonlinear Systems," *Journal of Guidance, Control, and Dynamics*, Vol. 20, No. 6, 1997, pp. 1083–1088.
[28] Marshall, A., and Tsiotras, P., "Spacecraft Angular Velocity Stabilization Using a Single-Gimbal Variable Speed Control Moment Gyro," AIAA Guidance, Navigation, and Control Conference, Austin, TX, AIAA Paper 2003-5654, Aug. 2003.
[29] Astolfi, A., and Ortega, R., "Energy-Based Stabilization of Angular Velocity of Rigid Body in Failure Configuration," *Journal of Guidance, Control, and Dynamics*, Vol. 25, No. 1, 2002, pp. 184–187.
[30] Aeyels, D., "On Stabilization by Means of the Energy-Casimir Method," *Systems and Control Letters*, Vol. 18, No. 5, 1992, pp. 325–328.
[31] Siguerdidjane, H. B., "A Possible New Way for Stabilizing by Smooth Feedback a Rigid Body Under Only One Control Torque," *Proceedings of the 31st IEEE Conference on Decision and Control* , Inst. of Electrical and Electronics Engineers, New York, Dec. 1992, pp. 1618–1619.
[32] Wan, C.-J., Coppola, V. T., and Bernstein, D. S., "A Lyapunov Function for the Energy-Casimir Method," *Proceedings of the 32nd IEEE Conference on Decision and Control* , Inst. of Electrical and Electronics Engineers, New York, 1993, pp. 3122–3123.
[33] Ahmed, J., and Bernstein, D. S., "Globally Convergent Adaptive Control of Spacecraft Angular Velocity Without Inertia Modeling," *Proceedings of the 1999 American Control Conference*, American Automatic Control Council, Evanston, IL, June 1999, pp. 1540–1544.
[34] Zuyev, A. L., "Application of Control Lyapunov Functions Technique for Partial Stabilization," *Proceedings of the 2001 IEEE International Conference on Control Applications*, Inst. of Electrical and Electronics Engineers, Piscataway, NJ, Sept. 2001, pp. 509–513.
[35] Bloch, A. M., Krishaprasad, P. S., Marsden, J. E., and Sanchez de Alvarez, G., "Stabilization of Rigid Body Dynamics by Internal and External Torques," *Automatica*, Vol. 28, No. 4, 1992, pp. 745–756.
[36] Kim, S., and Kim, Y., "Spin-Axis Stabilization of a Rigid Spacecraft Using Two Reaction Wheels," *Journal of Guidance, Control, and Dynamics*, Vol. 24, No. 5, 2001, pp. 1046–1049.
[37] Bloch, A. M., and Marsden, J. E., "Control and Stabilization of Systems with Heteroclinic Orbits," *Proceedings of the 31st IEEE Conference on Decision and Control* , Inst. of Electrical and Electronics Engineers, New York, Dec. 1989, pp. 2238–2242.
[38] Bloch, A. M., Leonard, N. E., and Marsden, J. E., "Stabilization of Mechanical Systems Using Controlled Lagrangians," *Proceedings of the 36th IEEE Conference on Decision and Control* , Inst. of Electrical and Electronics Engineers, Piscataway, NJ, 1997, pp. 2356–2361.
[39] Lum, K.-Y., and Bloch, A. M., "A Serret-Andoyer Transformation Analysis for the Controlled Rigid Body," *Proceedings of the 36th IEEE Conference on Decision and Control* , Inst. of Electrical and Electronics Engineers, Piscataway, NJ, Dec. 1997, pp. 3497–3502.
[40] Bloch, A. M., Leonard, N. E., and Marsden, J. E., "Matching and Stabilization by the Method of Controlled Lagrangians," *Proceedings of the 37th IEEE Conference on Decision and Control* , Inst. of Electrical and Electronics Engineers, Piscataway, NJ, Dec. 1998, pp. 1446–1451.
[41] Woolsey, C. A., Bloch, A. M., Leonard, N. E., and Marsden, J. E., "Dissipation and Controlled Euler-Poincare Systems," *Proceedings of the 40th IEEE Conference on Decision and Control* , Inst. of Electrical and Electronics Engineers, Piscataway, NJ, Dec. 2001, pp. 3378–3383.
[42] Kane, T. R., Likins, P. W., and Levinson, D. A., *Spacecraft Dynamics*, McGraw–Hill, New York, 1983.
[43] Hughes, P. C., *Spacecraft Attitude Dynamics*, Wiley, New York, 1986, pp. 66–68, 159, 178.
[44] Kane, T. R., and Levinson, D. A., *Dynamics: Theory and Applications*, McGraw–Hill, New York, 1985.
[45] Sidi, M. J., *Spacecraft Dynamics and Control*, Cambridge Aerospace Series, Vol. 7, Cambridge Univ. Press, New York, 1997.
[46] Slotine, J.-J. E., and Li, W., *Applied Nonlinear Control*, Prentice–Hall, Englewood Cliffs, 1991.
[47] Synge, J., and Griffith, B., *Principles of Mechanics*, 3rd ed., McGraw–Hill, New York, 1959.
[48] Wertz, J. (ed.), *Spacecraft Attitude Determination and Control*, Kluwer Academic, Norwell, MA, 1978.
[49] Thomson, W., *Introduction to Space Dynamics*, Dover Publications, Mineola, NY, 1986.
[50] Holden, T. E., and Lawrence, D. A., "A Lyapunov Design Approach to Nutation Damping with a Reaction Wheel," AIAA Conference on Guidance, Navigation and Control, Denver, CO, AIAA Paper 2000-4047, Aug. 2000.
[51] Bhat, S. P., and Bernstein, D. S., "Lyapunov Analysis of Semistability," *Proceedings of the 1999 American Control Conference*, American Automatic Control Council, Evanston, IL, June 1999, pp. 1608–1612.
[52] Vorotnikov, V. I., "On Two Classes of Partial Stability Problems," *PhysCon 2003*, Inst. of Electrical and Electronics Engineers, Piscataway, NJ, 2003, pp. 1141–1146.
[53] Meirovitch, L., *Methods of Analytical Dynamics*, McGraw–Hill, St. Louis, MO, 1970.
[54] Chobotov, V. A., *Spacecraft Attitude Dynamics and Control*, Krieger, Malabar, FL, 1991.
[55] Holden, T. E., and Lawrence, D. A., "A Lyapunov Approach to Magnetic Nutation Damping," AIAA Conference on Guidance, Navigation, and Control, Portland, OR, AIAA Paper 99-3971, Aug. 1999.
[56] Lew, A., Marsden, J. E., Ortiz, M., and West, M., "Variational Time Integrators," *International Journal for Numerical Methods in Engineering*, Vol. 60, No. 1, 2004, pp. 153–212.
[57] Chetayev, N. G., *Stability of Motion*, Pergamon, New York, 1961.
[58] Guckenheimer, J., and Holmes, P., *Nonlinear Oscillations, Dynamical Systems, and Bifurcations of Vector Fields*, Springer–Verlag, New York, 1983.